Effects of Doppler-Division Multiplexing on OFDM Joint Sensing and Communication Systems

OLIVER LANG [1] (Member, IEEE), **CHRISTIAN HOFBAUER** [2] (Member, IEEE), **REINHARD FEGER** [3],
AND MARIO HUEMER [1,4] (Member, IEEE)

[1]Institute of Signal Processing, Johannes Kepler University, 4040 Linz, Austria
[2]Silicon Austria Labs GmbH, 4040 Linz, Austria
[3]Institute for Communications Engineering and RF-Systems, Johannes Kepler University, 4040 Linz, Austria
[4]JKU LIT SAL eSPML Lab, 4040 Linz, Austria

CORRESPONDING AUTHOR: OLIVER LANG (email: oliver.lang@jku.at).

ABSTRACT A promising waveform candidate for future joint sensing and communication systems is orthogonal frequency-division multiplexing (OFDM). For such systems, supporting multiple transmit antennas requires multiplexing methods for the generation of orthogonal transmit signals, where equidistant subcarrier interleaving (ESI) is the most popular multiplexing method. In this work, we analyze a multiplexing method called Doppler-division multiplexing (DDM). This method applies a phase shift from OFDM symbol to OFDM symbol to separate signals transmitted by different Tx antennas along the velocity axis of the range-Doppler map. The main focus of this work lies on the implications of DDM on the communication task. It will be shown that for DDM, the channels observed in the communication receiver are heavily time-varying, preventing any meaningful transmission of data when not taken into account. In this work, a communication system designed to combat these time-varying channels is proposed, which includes methods for data estimation, synchronization, and channel estimation. Bit error ratio (BER) simulations demonstrate the superiority of this communications system compared to ESI-based systems.

INDEX TERMS Communication, multiplexing, OFDM, radar.

I. INTRODUCTION

Joint sensing and communication systems may be applied for automotive vehicle-to-vehicle communications and cellular sensing [1], [2], [3]. While many different system architectures are possible, a so-called dual-function radar-communication system is assumed in this work that uses the very same transmit signals for both, radar sensing and communications, simultaneously. A prominent waveform for joint sensing and communication systems is OFDM [4], [5], [6], [7], [8], which is also basis for the investigations in this work.

In many applications, multiple-input multiple-output (MIMO) systems [9] are employed to detect the angular positions of objects. These MIMO systems employ multiplexing methods for generating orthogonal transmit signals that are separable in the receiver. The most popular multiplexing method for the OFDM waveform is ESI [6], [10], for which each subcarrier is assigned to only one of the N_{Tx} Tx antennas. Hence, signals radiated by different Tx antennas can be separated in frequency domain. Several extensions of ESI exist with randomly allocated subcarriers [11], with non-equidistantly allocated subcarriers [7], and with dynamically allocated subcarriers [12]. The latter one is referred to as non-equidistant dynamic subcarrier interleaving (NeqDySI), and it changes the allocation of the subcarriers onto the Tx antennas from OFDM symbol to OFDM symbol.

Another relevant multiplexing method is auto-correlation-based code-division multiplexing (AC-CDM) [13]. For this method, the same data are radiated on every Tx antenna and on every subcarrier except for antenna-specific time delays. These time delays move the corresponding receive signals along the range axis of the range-Doppler map (RDM) such that N_{Tx} peaks appear along the range axis for each real object.

The multiplexing method analyzed in [13] is denoted as modified repeated symbol CDM (MRS-CDM), which applies orthogonal Hadamard codes onto the OFDM symbols transmitted by different Tx antennas. In the receiver, N_{Tx} RDMs are evaluated separately, one for each Tx antenna. In every RDM there appears one main peak and $N_{Tx} - 1$ spurs along the velocity axis for each real object such that the maximum unambiguous velocity is reduced by a factor of N_{Tx}.

The discrete Fourier transform (DFT)-coded multiplexing method investigated in [14] applies a DFT matrix as precoding matrix onto the transmit signals that shifts the corresponding receive signals either along the range axis, the velocity axis, or both of them.

The multiplexing method analyzed in [15] is referred to as range-division multiplexing (RDMult), and it applies a phase shift from subcarrier to subcarrier to shift the signal components of the RDM along the range axis.

This work focuses on a multiplexing method referred to as DDM. DDM modifies the transmit signal for each of the N_{Tx} Tx antenna such that the received signal components are shifted along the velocity axis. The signal component radiated by different Tx antennas can thus simply be separated by dividing the RDM in N_{Tx} areas along the velocity axis. For radar sensing, the performance in terms of the signal-to-noise ratio (SNR) in the RDM of a MIMO OFDM radar system utilizing DDM is approximately equal to a MIMO OFDM radar system employing ESI.

Note that DDM shares some similarities with the DFT-coded multiplexing method [14] and with MRS-CDM [13], which spread signal components from different Tx antennas along the velocity axis, too. However, these multiplexing techniques were not analyzed regarding their implications for communications. Consequently, this work focuses on the effects of DDM on the communication task of a joint sensing and communication system, leading to the following novel contributions of this work.

- It will be shown that a so-called effective channel, which is a single-input single-output (SISO) channel although several transmit antennas are involved, sufficiently models the communication channel.
- It will be shown that the specific design of the transmit signal for DDM affects the effective channel. More specifically, it will turn out that the effective channel is affected by constructive or destructive interference, which is a typical effect for MIMO systems. However, the special transmit signals for DDM cause the effective channel to be heavily time-varying. As a consequence, the channel coefficients may significantly change in

magnitude and phase from one OFDM symbol to the next one.
- A comprehensive analysis of this observation is presented, which reveals that the constructive or destructive interference for the effective channel appears in a certain repeating pattern.
- A communication system capable of dealing with these time-varying effective channels is proposed in this work. This communication system includes methods for synchronization, channel estimation, and data estimation.
- The communication system's performance is evaluated via extensive BER simulations.

It will turn out that a joint sensing and communication system using DDM performs very similar to a system utilizing RDMult. However, it makes sense to choose DDM over RDMult for some applications due to different trade-offs being made regarding the maximum unambiguous velocity v_{max} and the maximum unambiguous range r_{max}. In case DDM is preferred, this work presents a detailed analysis of the implications of DDM on communications and suitable signal processing methods.

Organization: Section II recaps the radar signal model. The DDM method is described in Section III. The proposed communication system for a DDM OFDM waveform is explained in Section IV, and Section V analyzes the BER simulation results of this system. This work is concluded in Section VI.

Notation and Definitions: Vectors and matrices are indicated by lower-case and upper-case bold face variables, respectively. The element of a matrix at its lth row and kth column is defined as $[\mathbf{A}]_{l,k}$, where the indices start with 0. $\mathbb{R}$ and $\mathbb{C}$ represent the set of real and complex values, respectively. A superscript to $\mathbb{R}$ or $\mathbb{C}$ indicates the dimensions. Moreover, j represents the imaginary unit, $(\cdot)^T$ denotes the transposition, $(\cdot)^H$ represents the conjugate transposition, $(\cdot)^*$ indicates complex conjugation. The identity matrix of size $n \times n$ is denoted as $\mathbf{I}^n$, and a column vector of length n with all elements equal to 1 is indicated by $\mathbf{1}^n$. The Hadamard product is represented by $\odot$. $\mathbf{F}_N$ represents the DFT matrix of size $N \times N$ with $[\mathbf{F}_N]_{l,k} = \exp(-j2\pi lk/N)$ and $l, k = 0, \ldots, N - 1$. The vector $\mathbf{d}_N(f) \in \mathbb{C}^N$ is defined as $\mathbf{d}_N(f) = \begin{bmatrix} 1 & e^{j2\pi f} & \ldots & e^{j2\pi f(N-1)} \end{bmatrix}^T$, with f being a unitless placeholder variable. The matrix $\mathbf{D}_N(f) \in \mathbb{C}^{N \times N}$ is a diagonal matrix defined as $\mathbf{D}_N(f) = \text{diag}(\mathbf{d}_N(f))$.

II. RADAR SIGNAL MODEL

Cyclic prefix (CP)-OFDM (simply referred to as OFDM) is widely adopted in wireless communications [16] and the reader is thus expected to be familiar with it. This section briefly recaps the OFDM signal model in complex baseband from [8], [15]. The derivation of this signal model considers only a single Rx antenna, while a possible extension to multiple Rx antennas can be easily adapted. Note that the channel within this signal model represents a typical radar channel model and will only be used for the explanations concerning the radar sensing part of this work, while a typical

communication channel model will be used for the investigations concerning the communication part.

In the following, f_c denotes the carrier frequency, B refers to the bandwidth, N_c is the number of subcarriers, N_{sym} is the number of OFDM symbols, $\Delta f = B/N_c$ is the subcarrier spacing, and T_{cp} denotes the length of the CP. Let the matrices $\mathbf{S}_k \in \mathbb{C}^{N_c \times N_{sym}}$ with $k = 0, 1, \ldots, N_{Tx} - 1$ contain the transmit subcarrier symbols for all N_{Tx} Tx antennas and all N_{sym} OFDM symbols. The transmit signal in complex baseband is derived by transforming these OFDM symbols into time domain and extending them with a CP.

The channel between transmitter and receiver assumes N_{path} propagation paths between each of the N_{Tx} Tx antennas and the Rx antenna with $r_{i,k}$ denoting the propagation distance for the kth Tx antenna along the ith path. $\tau_{i,k} = 2r_{i,k}/c_0$ is the corresponding round-trip delay time and can be normalized to $\bar{\tau}_{i,k} = \tau_{i,k}\Delta f$ and with c_0 denoting the speed of light. $a_i \in \mathbb{C}$ models assumed constant amplitude and phase changes during propagation along the ith path [8].

At the receiver, the time domain analog-to-digital converter (ADC) samples are stored in a matrix $\mathbf{Y}_{tf,ts} \in \mathbb{C}^{N_c \times N_{sym}}$, where every column corresponds to a received OFDM symbol in time domain and without the CP. This matrix $\mathbf{Y}_{tf,ts}$ is given by [8], [15]

$$\mathbf{Y}_{tf,ts} = \sum_{k=0}^{N_{Tx}-1} \sum_{i=0}^{N_{path}-1} \bar{a}_{i,k} \mathbf{D}_{N_c}\left(\frac{\bar{f}_{D_i}}{N_c}\right) \mathbf{F}_{N_c}^{-1} \mathbf{D}_{N_c}^*(\bar{\tau}_{i,k})$$
$$\cdot \mathbf{S}_k \mathbf{D}_{N_{sym}}(\bar{f}_{D_i}\alpha) + \mathbf{N}, \tag{1}$$

where $\mathbf{N} \in \mathbb{C}^{N_c \times N_{sym}}$ models additive measurement noise, and where 'tf' and 'ts' indicate the fast time and the slow time over the vertical and horizontal matrix dimensions, respectively. Additionally, we used $\bar{a}_{i,k} = a_i \exp(-j2\pi f_c \tau_{i,k}) \in \mathbb{C}$ and $\alpha = (1/\Delta f + T_{cp})\Delta f \in \mathbb{R}$. The Doppler shift along the ith path caused by a relative velocity v_i is defined as $f_{D_i} = -2v_i f_c/c_0$, and it is normalized to $\bar{f}_{D_i} = f_{D_i}/\Delta f$. The implications of the Doppler shift are considered in the form of a common phase error (CPE) and inter-carrier interference (ICI) affecting the received OFDM symbols. The CPE and ICI are represented in (1) in the form of $\mathbf{D}_{N_{sym}}(\bar{f}_{D_i}\alpha)$ and $\mathbf{D}_{N_c}(\frac{\bar{f}_{D_i}}{N_c})$, respectively.

The receiver senses signals reflected from objects and feeds them into the standard radar receiver signal processing chain detailed, e.g., in [4], [5], [15].

In case several receive antennas are considered, a similar matrix as in (1) can be constructed for every Rx antenna with appropriately modified parameters $\bar{a}_{i,k}$ and $\bar{\tau}_{i,k}$ that model the amplitude change and the delay along the paths between each Tx antenna and each Rx antenna [13], [14].

III. DOPPLER-DIVISION MULTIPLEXING

The key aspect of DDM is a modification of the individual transmit signals for every Tx antenna such that the corresponding receive signals are shifted along the velocity axis in the RDM. These modified transmit signals are discussed in the following.

For the signal model in (1), a shift along the velocity axis in the RDM is implemented by applying a phase shift from OFDM symbol to OFDM symbol. This phase shift is denoted as $\Delta\psi_k$ for $0 \leq k < N_{Tx}$. Applying this phase shift in the transmitter is achieved by choosing $\mathbf{S}_k$ in (1) to be

$$\mathbf{S}_k = \mathbf{S}\mathbf{D}_{N_{sym}}\left(\frac{\Delta\psi_k}{2\pi}\right). \tag{2}$$

The transmit signals in time domain are again obtained by transforming these OFDM symbols into time domain and extending them with a CP.

Note that $\mathbf{S}$, and thus the payload, is the same for all Tx antennas. Only the modulation by $\mathbf{D}_{N_{sym}}(\frac{\Delta\psi_k}{2\pi})$ makes them distinguishable from each other. The processing chain in the radar receiver comprises the standard radar receiver processing steps detailed, e.g., in [4], [5], [15].

The shift of the signal components along the velocity axis is determined by $\Delta\psi_k$. It is recommended to choose $\Delta\psi_k = 2\pi\frac{p}{N_{sym}}$ for any $p \in \mathbb{Z}$, which circularly shifts the corresponding signal components by p velocity bins without changing the magnitude or phase values. This statement can be proven by a straightforward modification of a related proof in [15]. Since no distortions of the magnitude or phase values are induced, a utilization of them for digital beamforming (DBF) [17] is easily possible.

Furthermore, for $N_{Tx} = 4$, it is easy to prove that the choice $\Delta\psi_k = \{-\frac{3\pi}{4}, -\frac{\pi}{4}, \frac{\pi}{4}, \frac{3\pi}{4}\}$ separates the RDM in 4 equally sized areas. Thus, it will be the primary choice for $\Delta\psi_k$ in this work, and it entails the necessity of reducing the maximum unambiguous velocity v_{max} by a factor of $N_{Tx} = 4$.

Further details concerning DDM are discussed in the following.

- Employing a DFT precoding matrix of size $N_{Tx} \times N_{Tx}$ as utilized in [14] may produce the same phase shift values as used in this work, however, it offers less freedom in choosing the shift along the velocity axis.
- Performing the same SNR analysis as in [15] for DDM reveals that approximately the same SNR in the RDM is obtained for DDM as for ESI and RDMult.
- The computational complexity for implementing DDM on the transmitter side is the very same as for RDMult, but it is in general higher than for implementing ESI.

IV. COMMUNICATION SYSTEM BASED ON DDM

The DDM method generates transmit signals designed for multiplexing purposes in radar sensing applications. The effects of the transmit signal design due to DDM on the communication task are investigated in this section. Based on these investigations, a communication system specifically designed for DDM is proposed. In the following, the terms 'receiver' and 'Rx antenna' do not refer to the radar receiver but to the communication receiver.

For these investigations, the waveform and system parameters are chosen according to Table 1. The communication receiver employs only a single Rx antenna (multiple-input single-output (MISO)), which will turn out to be sufficient
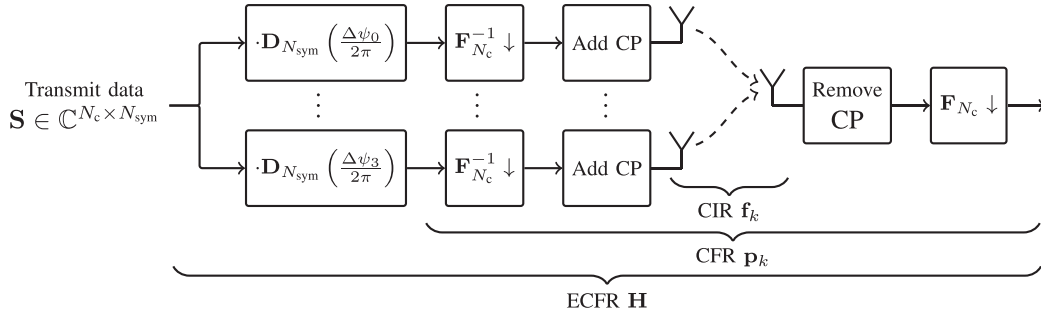
FIGURE 1. Transmitter and receiver processing chains including the CIR, the CFR, and the ECFR with their covered processing blocks. The parallel-to-serial conversions, the DACs, the ADC, and the analog front-ends are not shown for simplicity. The figure is based on a similar figure in [15].

TABLE 1. Waveform and System Parameters

Parameter	Value
Carrier frequency f_c	77 GHz
Bandwidth B	1 GHz
Number of subcarriers N_c	1024
Length of the cyclic prefix T_{cp}	1 µs
Number of OFDM symbols N_{sym}	512
Number of Rx antennas N_{Rx}	1
Number of Tx antennas N_{Tx}	4
Symbol alphabet	QPSK
Phase shift $\Delta\psi_k$	$\{-\frac{3\pi}{4}, -\frac{\pi}{4}, \frac{\pi}{4}, \frac{3\pi}{4}\}$

for enabling communications. An extension to multiple Rx antennas is straightforward.

A. CHANNEL MODEL

Fig. 1 shows the processing blocks for DDM in the transmitter, the N_{Tx} channel impulse responses (CIRs) from each Tx antenna to the Rx antenna, and the first two receiver processing blocks. On the basis of that, we will discuss different channel representations.

1) CIR AND CFR REPRESENTATION

A straightforward way of describing the channel is to utilize the N_{Tx} individual CIRs. The utilized model for these CIRs is described in [18], [19], [20], [21], [22], [23] and code for automated generation of random CIRs is provided in [24] for which we used the same parametrization as employed in [15]. These CIRs are denoted as $f_k \in \mathbb{C}^{N_f}$ for $0 \le k < N_{Tx}$ and their assumed length is $N_f = 256$. The linear convolution with the CIRs transform into a circular convolution for the time domain signal without the CP, which can be described by a multiplication with the channel frequency responses (CFRs)

$$\mathbf{p}_k = \mathbf{F}_{N_c} \mathbf{B}_{zp} \mathbf{f}_k \quad (3)$$

in frequency domain, whereas the matrix $\mathbf{B}_{zp} \in \mathbb{C}^{N_c \times N_f}$ zero-pads the CIRs $\mathbf{f}_k$ to a length of N_c.

2) ECFR REPRESENTATION

Here, we exploit the fact that all antennas transmit the same subcarrier symbols $\mathbf{S}$ up to the deterministic phase shift $\Delta\psi_k$. This allows for introducing a channel that covers all shown processing blocks in Fig. 1. This channel representation is referred to as effective channel frequency response (ECFR), which can be modeled as a SISO channel even though several Tx antennas are involved.

As depicted in Fig. 1, the ECFR covers the CFRs and the diagonal matrices $\mathbf{D}_{N_{sym}}(\frac{\Delta\psi_k}{2\pi})$. These diagonal matrices apply a phase shift from OFDM symbol to OFDM symbol. Thus, the ECFR will change from OFDM symbol to OFDM symbol. Let $\mathbf{H} \in \mathbb{C}^{N_c \times N_{sym}}$ denote the ECFR for all N_{sym} OFDM symbols, then, $\mathbf{H}$ is given by

$$\mathbf{H} = \sum_{k=0}^{N_{Tx}-1} \mathbf{Q}_k, \quad (4)$$

where the matrices $\mathbf{Q}_k \in \mathbb{C}^{N_c \times N_{sym}}$ are given as

$$\mathbf{Q}_k = \mathbf{p}_k \left(\mathbf{1}^{N_{sym}}\right)^T \mathbf{D}_{N_{sym}} \left(\frac{\Delta\psi_k}{2\pi}\right) = \mathbf{p}_k \mathbf{d}_{N_{sym}} \left(\frac{\Delta\psi_k}{2\pi}\right)^T. \quad (5)$$

Each matrix $\mathbf{Q}_k$ for $0 \le k < N_{Tx}$ represents one signal path in Fig. 1.

3) PROPERTIES OF THE ECFR

Note that the N_{Tx} different terms used to construct the ECFR in (4) may interfere constructively or destructively. On top of that, this constructive/destructive interference turns out to be heavily time-varying.

The time-dependent constructive/destructive interference of the ECFR in (4) can be well demonstrated for additive white Gaussian noise (AWGN) channels for which $\mathbf{Q}_k$ in (5) reduces to

$$\mathbf{Q}_k = \mathbf{1}^{N_c} \mathbf{d}_{N_{sym}} \left(\frac{\Delta\psi_k}{2\pi}\right)^T. \quad (6)$$

According to (6), all subcarriers experience the same effects. It is thus sufficient to inspect a single subcarrier, e.g, the first one, whose channel coefficient rotates along the unit circle. This subcarrier is represented by the first row of $\mathbf{Q}_k$
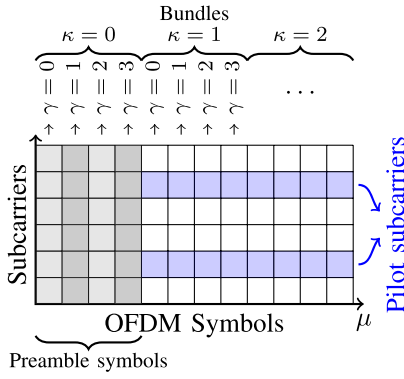
TABLE 2. Schematic Visualization of the Elements of $[\mathbf{Q}_k]_{0,\mu}$ for $0 \leq k < N_{\text{Tx}}$ and for $0 \leq \mu < 9$ in the Case of AWGN Channels

μ	0	1	2	3	4	5	6	7	8
$[\mathbf{Q}_0]_{0,\mu}$	→	↙	↑	↘	←	↗	↓	↖	→
$[\mathbf{Q}_1]_{0,\mu}$	→	↘	↓	↙	←	↖	↑	↗	→
$[\mathbf{Q}_2]_{0,\mu}$	→	↗	↑	↖	←	↙	↓	↘	→
$[\mathbf{Q}_3]_{0,\mu}$	→	↖	↓	↗	←	↘	↑	↙	→
$[\mathbf{H}]_{0,\mu}$	⟶	0	0	0	⟵	0	0	0	⟶

FIGURE 2. Normalized power of the first subcarrier of an exemplary frequency selective ECFR plotted over the OFDM symbol index μ.

denoted as $[\mathbf{Q}_k]_{0,\mu}$, where the OFDM symbols are indexed with $0 \leq \mu < N_{\text{sym}}$. The magnitude and phase values for these elements in case of AWGN channels are exemplarily sketched in form of arrows in the complex plane in Table 2 for the first 9 OFDM symbols $0 \leq \mu < 9$ and for the choice of $\Delta\psi_k = \{\frac{\pi}{4}, \frac{3\pi}{4}, \frac{5\pi}{4}, \frac{7\pi}{4}\}$. According to (4), the sum of the elements $[\mathbf{Q}_k]_{0,\mu}$ for $0 \leq k < N_{\text{Tx}}$ yields the first subcarrier of the ECFR $[\mathbf{H}]_{0,\mu}$ for the μth OFDM symbol, which is also sketched in Table 2. One can see, that for $\mu = 0$ all components add up constructively. Hence, the ECFR can be considered to be good and the received signal power will be maximized for this OFDM symbol. The next three OFDM symbols observe destructive interference leading to full cancellation of the signal components, such that the received signal power is zero. For the OFDM symbols $\mu = 4, \ldots 7$ the arrows point in the opposite direction than for $\mu = 0, \ldots 3$, respectively. This pattern repeats for $\mu \geq 8$. For the AWGN case, we notice that constructive/destructive interference is observed with a period of 8 OFDM symbols. Within this period, the ECFR for the first 4 OFDM symbols equals that for the subsequent 4 OFDM symbols when inverting all signs.

The same analysis for the employed frequency selective CIR model is presented in the following. For this model, the magnitude values of $[\mathbf{H}]_{0,\mu}$ for an exemplary ECFR are shown in Fig. 2. Since the real-valued magnitude rather than the complex-valued amplitude values are shown, a period of 4 OFDM symbols is observed. Within these 4 OFDM symbols, one can observe a pattern where 3 OFDM symbols experience a rather strong attenuation, making a successful transmission difficult. Consequently, robustifying communication is necessary.

4) INCREASING ROBUSTNESS OF THE COMMUNICATION

In wireless communications, bad channel conditions are usually tackled by adding redundancy to the transmit data. We propose adding redundancy to the transmit data by sending the same subcarrier symbols on 4 consecutive OFDM symbols in combination with a channel code with a code rate of $r = 1/2$. The former can be implemented with very low complexity and is inspired by space-time codes [25], [26], [27], which utilize diversity gain to robustify the transmission in difficult environments. The proposed approach also utilizes diversity gain, which will result in an increased BER performance compared to, e.g., ESI as will be shown later in this work. It shall be noted that this increase in BER performance comes at the cost of a reduced data rate. Transmitting the same subcarrier symbols on 4 consecutive OFDM symbols is mathematically described by constructing $\mathbf{S}$ according to

$$\mathbf{S} = \mathbf{XB}, \tag{7}$$

with $\mathbf{B}$ given as

$$\mathbf{B} = \begin{bmatrix} 1\,1\,1\,1\,0\,0\,0\,0\,0\,0\,0\,0 & 0\,0\,0\,0 \\ 0\,0\,0\,0\,1\,1\,1\,1\,0\,0\,0\,0 \ldots & 0\,0\,0\,0 \\ 0\,0\,0\,0\,0\,0\,0\,0\,1\,1\,1\,1 & 0\,0\,0\,0 \\ \vdots \quad \vdots \quad \vdots \quad \ddots \quad \vdots \\ 0\,0\,0\,0\,0\,0\,0\,0\,0\,0\,0\,0 \ldots & 1\,1\,1\,1 \end{bmatrix} \in \mathbb{R}^{(N_{\text{sym}}/4) \times N_{\text{sym}}}. \tag{8}$$

This way, the subcarrier symbols in every column in $\mathbf{X} \in \mathbb{C}^{N_{\text{c}} \times N_{\text{sym}}/4}$ are spread over 4 consecutive OFDM symbols in $\mathbf{S}$.

B. COMMUNICATION SIGNAL MODEL

The communication signal model is similar to (1) except that it applies to the communication receiver rather than the radar receiver. Hence, it uses the ECFR discussed for the communication task. Moreover, for reasons of compactness of the subsequent mathematical derivations, we do not consider ICI in the model since the proposed communication receiver does not counteract this effect anyway. However, ICI is fully considered for all simulations in this work.

For the mathematical description, 4 consecutive OFDM symbols within $\mathbf{S}$ carrying the same subcarrier symbols are referred to as a bundle. Hence, $\mathbf{S}$ contains $N_{\text{sym}}/4$ bundles indexed with $0 \leq \kappa < N_{\text{sym}}/4$. Within every bundle, the 4 OFDM symbols are indexed with $0 \leq \gamma < 4$. This notation is visualized in Fig. 3, which sketches the rows and columns of $\mathbf{S}$. The columns of $\mathbf{S}$ are denoted as $\mathbf{s}_{\kappa,\gamma} \in \mathbb{C}^{N_{\text{c}}}$ with κ and γ indicating the corresponding bundle and the OFDM symbol within this bundle, respectively. The columns of the matrix $\mathbf{X}$ are denoted as $\mathbf{x}_\kappa \in \mathbb{C}^{N_{\text{c}}}$. This way, it holds that $\mathbf{x}_\kappa = \mathbf{s}_{\kappa,\gamma}$ for $0 \leq \gamma < 4$. With $\mathbf{P}_k = \text{diag}(\mathbf{p}_k)$, (2), (4), (5), and (7), the communication signal model is

FIGURE 3. Exemplary allocation of preamble OFDM symbols and pilot subcarriers in $\mathbf{S}$ for DDM.

given by

$$\mathbf{Y}_{\text{tf,ts}} = \sum_{k=0}^{N_{\text{Tx}}-1} \mathbf{F}_{N_\text{c}}^{-1} \mathbf{P}_k \mathbf{S}_k \boldsymbol{\Lambda} + \mathbf{N} \tag{9}$$

$$= \sum_{k=0}^{N_{\text{Tx}}-1} \mathbf{F}_{N_\text{c}}^{-1} \mathbf{P}_k \mathbf{S} \mathbf{D}_{N_{\text{sym}}} \left(\frac{\Delta \psi_k}{2\pi} \right) \boldsymbol{\Lambda} + \mathbf{N} \tag{10}$$

$$= \mathbf{F}_{N_\text{c}}^{-1} \left(\mathbf{H} \odot \mathbf{S} \right) \boldsymbol{\Lambda} + \mathbf{N} \tag{11}$$

$$= \mathbf{F}_{N_\text{c}}^{-1} \left(\mathbf{H} \odot (\mathbf{XB}) \right) \boldsymbol{\Lambda} + \mathbf{N}. \tag{12}$$

The diagonal matrix $\boldsymbol{\Lambda} \in \mathbb{C}^{N_{\text{sym}} \times N_{\text{sym}}}$ models the CPEs. Its diagonal elements are given by $e^{j\varphi_{\kappa,\gamma}}$ with $\varphi_{\kappa,\gamma}$ representing the unknown CPE for the γth OFDM symbol within the κth bundle. The matrix $\mathbf{N} \in \mathbb{C}^{N_\text{c} \times N_{\text{sym}}}$ represents zero-mean white Gaussian measurement noise, whose uncorrelated elements have a variance of σ_{n}^2.

Recall that the ECFR $\mathbf{H}$ shows a period of 8 columns. Within this period, the columns of $\mathbf{H}$ show a pattern where the first 4 columns are equal with the following 4 columns when inverting all signs. This pattern is accounted for by inverting the signs of the received signals for the corresponding OFDM symbols as described in the following. Let $\mathbf{y}_{\kappa,\gamma} \in \mathbb{C}^{N_\text{c}}$ be the column of $\mathbf{Y}_{\text{tf,ts}}$ corresponding to the γth OFDM symbol within the κth bundle, and let $\mathbf{z}_{\kappa,\gamma} \in \mathbb{C}^{N_\text{c}}$ be its DFT transform up to a sign inversion in case of odd values of κ

$$\mathbf{z}_{\kappa,\gamma} = (-1)^\kappa \mathbf{F}_{N_\text{c}} \mathbf{y}_{\kappa,\gamma}. \tag{13}$$

The follow-up receiver signal processing is based on $\mathbf{z}_{\kappa,\gamma}$ rather than on $\mathbf{y}_{\kappa,\gamma}$, which allows describing the ECFR $\mathbf{H}$ by only 4 columns. These 4 columns will be denoted as $\mathbf{h}_\gamma \in \mathbb{C}^{N_\text{c}}$ for $\gamma = 0, \ldots, 3$. From now on, these 4 vectors are referred to as ECFR for the sake of simplicity. A diagonal matrix with the ECFR is defined as $\mathbf{H}_\gamma = \text{diag}(\mathbf{h}_\gamma) \in \mathbb{C}^{N_\text{c} \times N_\text{c}}$.

The ECFR $\mathbf{h}_\gamma$ transformed into the time domain is denoted as effective channel impulse response (ECIR) $\mathbf{g}_\gamma \in \mathbb{C}^{N_\mathbf{g}}$, whose length $N_\mathbf{g}$ corresponds to the length of the CIR $\mathbf{f}_k$ of $N_\mathbf{f} = N_\mathbf{g} = 256$. The ECIR and the ECFR are connected

via

$$\mathbf{h}_\gamma = \mathbf{F}_{N_\text{c}} \mathbf{B}_{\text{zp}} \mathbf{g}_\gamma. \tag{14}$$

The introduced definitions and notations allow simplifying the model in (9)–(12) as

$$\mathbf{z}_{\kappa,\gamma} = \mathbf{H}_\gamma \mathbf{s}_{\kappa,\gamma} e^{j\varphi_{\kappa,\gamma}} + \mathbf{n}_{\kappa,\gamma} \tag{15}$$

$$= \mathbf{H}_\gamma \mathbf{x}_\kappa e^{j\varphi_{\kappa,\gamma}} + \mathbf{n}_{\kappa,\gamma}, \tag{16}$$

where $\mathbf{n}_{\kappa,\gamma} \in \mathbb{C}^{N_\text{c}}$ is a white Gaussian noise vector given by the DFT of the corresponding columns of $\mathbf{N}$. The alternating sign considered in (13) is ignored for the noise since it does not affect its statistics. The covariance matrix of $\mathbf{n}_{\kappa,\gamma}$ is given by $\mathbf{C_{nn}} = N_\text{c} \sigma_{\text{n}}^2 \mathbf{I}^{N_\text{c}}$.

The matrix $\mathbf{S}$ contains N_{pr} preamble OFDM symbols in the first N_{pr} columns, which are used for channel estimation later in this work. Thus, $\mathbf{X}$ contains $N_{\text{pr}}/4$ preamble OFDM symbols in the first $N_{\text{pr}}/4$ columns, where it is assumed that N_{pr} is a multiple of 4. Let $\mathbf{x}_{\text{pr}} \in \mathbb{C}^{N_\text{c}}$ be the preamble OFDM symbol in frequency domain such that $\mathbf{x}_\kappa = \mathbf{x}_{\text{pr}}$ for $0 \leq \kappa < N_{\text{pr}}/4$.

For $\kappa \geq N_{\text{pr}}/4$, $\mathbf{x}_\kappa$ consists of N_p pilot and N_d data subcarriers such that $N_\text{c} = N_\text{p} + N_\text{d}$. The symbols transmitted on the pilot subcarriers are known to the receiver and are used for synchronization. The variance of the assumed uncorrelated data subcarriers is denoted as σ_d^2, which is usually normalized such that $\sigma_\text{d}^2 = 1$.

Dividing subcarriers into data subcarriers and pilot subcarriers not only applies to $\mathbf{x}_\kappa$ but also to many other variables such as $\mathbf{s}_{\kappa,\gamma}$, $\mathbf{z}_{\kappa,\gamma}$, $\mathbf{n}_{\kappa,\gamma}$, $\mathbf{h}_\gamma$, and $\mathbf{H}_\gamma$. In the following, the superscript 'p' indicates the pilot subcarriers only, and the superscript 'd' refers to the data subcarriers only.

C. CHANNEL ESTIMATION
The OFDM preamble symbols are utilized for channel estimation. As a preparatory step, these symbols are synchronized to account for a potential CPE, e.g., caused by a relative velocity between transmitter and receiver.

1) SYNCHRONIZATION OF THE PREAMBLE OFDM SYMBOLS
The model in (16) serves as a basis for synchronization, however, as usual in channel estimation, the roles of the channel and the preamble OFDM symbols are reversed. This yields

$$\mathbf{z}_{\kappa,\gamma} = \mathbf{X}_{\text{pr}} \mathbf{h}_\gamma e^{j\varphi_{\kappa,\gamma}} + \mathbf{n}_{\kappa,\gamma}, \tag{17}$$

where $\mathbf{X}_{\text{pr}} = \text{diag}(\mathbf{x}_{\text{pr}}) \in \mathbb{C}^{N_\text{c} \times N_\text{c}}$. Without loss of generality, $\varphi_{0,\gamma}$ is set to 0 and we estimate the CPE within $\mathbf{z}_{\kappa,\gamma}$ with respect to $\mathbf{z}_{0,\gamma}$ via $\widehat{\varphi}_{\kappa,\gamma} = \arg(\mathbf{z}_{0,\gamma}^H \mathbf{z}_{\kappa,\gamma})$ [28], [29], whereas $\widehat{\cdot}$ indicates that $\widehat{\varphi}_{\kappa,\gamma}$ is an estimate of $\varphi_{\kappa,\gamma}$. This estimation procedure is repeated for $0 \leq \gamma < 4$ and $0 \leq \kappa < N_{\text{pr}}/4$. The estimated CPEs are then used to synchronize $\mathbf{z}_{\kappa,\gamma}$ and averaged within one bundle, yielding

$$\bar{\mathbf{z}}_\gamma = \frac{1}{N_{\text{pr}}/4} \sum_{\kappa=0}^{N_{\text{pr}}/4-1} \mathbf{z}_{\kappa,\gamma} e^{-j\widehat{\varphi}_{\kappa,\gamma}}. \tag{18}$$

With (14) and (18), (17) can be approximated by

$$\bar{\mathbf{z}}_\gamma \approx \underbrace{\mathbf{X}_{\mathrm{pr}}\mathbf{F}_{N_{\mathrm{c}}}\mathbf{B}_{\mathrm{zp}}}_{\mathbf{M}_{\mathrm{pr}}}\mathbf{g}_\gamma + \underbrace{\frac{1}{N_{\mathrm{pr}}/4}\sum_{\kappa=0}^{N_{\mathrm{pr}}/4-1}\mathbf{n}_{\kappa,\gamma}}_{\mathbf{n}_\gamma} \qquad (19)$$

$$= \mathbf{M}_{\mathrm{pr}}\mathbf{g}_\gamma + \mathbf{n}_\gamma. \qquad (20)$$

2) ECIR/ECFR ESTIMATION

Employing the commonly used best linear unbiased estimator (BLUE) [30], [31], [32], [33] for estimating the ECIR $\mathbf{g}_\gamma$ in (20), and transforming the result into an estimate of the corresponding ECFRs yields

$$\widehat{\mathbf{H}}_\gamma = \mathrm{diag}\left(\widehat{\mathbf{h}}_\gamma\right) = \mathrm{diag}\left(\mathbf{F}_{N_{\mathrm{c}}}\mathbf{B}_{\mathrm{zp}}\left(\mathbf{M}_{\mathrm{pr}}^H\mathbf{M}_{\mathrm{pr}}\right)^{-1}\mathbf{M}_{\mathrm{pr}}^H\bar{\mathbf{z}}_\gamma\right).$$

This procedure is repeated for all indexes $\gamma = 0, \ldots, 3$. Note that the matrix inverse can be precomputed since it only depends on the usually constant preamble OFDM symbols.

D. SYNCHRONIZATION OF OFDM SYMBOLS FOR $\kappa \geq N_{PR}/4$

Considering only the pilot subcarriers of the model in (15) and replacing the ECFR by its estimate yields

$$\mathbf{z}_{\kappa,\gamma}^{\mathrm{p}} \approx \widehat{\mathbf{H}}_\gamma^{\mathrm{p}}\underbrace{\mathbf{s}_{\kappa,\gamma}^{\mathrm{p}}\mathrm{e}^{\mathrm{j}\varphi_{\kappa,\gamma}}}_{\mathbf{t}_{\kappa,\gamma}^{\mathrm{p}}} + \mathbf{n}_{\kappa,\gamma}^{\mathrm{p}} = \widehat{\mathbf{H}}_\gamma^{\mathrm{p}}\mathbf{t}_{\kappa,\gamma}^{\mathrm{p}} + \mathbf{n}_{\kappa,\gamma}^{\mathrm{p}}, \qquad (21)$$

where $\mathbf{t}_{\kappa,\gamma}^{\mathrm{p}} = \mathbf{s}_{\kappa,\gamma}^{\mathrm{p}}\mathrm{e}^{\mathrm{j}\varphi_{\kappa,\gamma}} \in \mathbb{C}^{N_{\mathrm{p}}}$ represents CPE distorted pilot symbols [34], [35]. Employing the commonly used linear minimum mean square error (LMMSE) estimator [15], [28], [29], [30], [33], [36] on (21) yields

$$\widehat{\mathbf{t}}_{\kappa,\gamma}^{\mathrm{p}} = \left(\left(\widehat{\mathbf{H}}_\gamma^{\mathrm{p}}\right)^H\widehat{\mathbf{H}}_\gamma^{\mathrm{p}} + N_{\mathrm{c}}\sigma_{\mathrm{n}}^2\mathbf{C}_{\mathbf{tt}}^{-1}\right)^{-1}\left(\widehat{\mathbf{H}}_\gamma^{\mathrm{p}}\right)^H\mathbf{z}_{\kappa,\gamma}^{\mathrm{p}}. \qquad (22)$$

There, $\mathbf{C}_{\mathbf{tt}} \in \mathbb{C}^{N_{\mathrm{p}}\times N_{\mathrm{p}}}$ denotes the covariance matrix of $\mathbf{t}_{\kappa,\gamma}^{\mathrm{p}}$ and it is assumed to be a diagonal matrix for simplicity. The diagonal elements of $\mathbf{C}_{\mathbf{tt}}$ represent the pilot symbols' average power (averaged over the OFDM symbols). Comparing the estimates $\widehat{\mathbf{t}}_{\kappa,\gamma}^{\mathrm{p}}$ in (22) with the known transmitted pilot symbols $\mathbf{s}_{\kappa,\gamma}^{\mathrm{p}}$ allows estimating the CPE for every $\kappa \geq N_{\mathrm{pr}}/4$ and for $0 \leq \gamma < 4$ according to $\widehat{\varphi}_{\kappa,\gamma} = \arg((\mathbf{s}_{\kappa,\gamma}^{\mathrm{p}})^H\mathbf{W}\widehat{\mathbf{t}}_{\kappa,\gamma}^{\mathrm{p}})$ [28], [29]. Here, the optional diagonal matrix $\mathbf{W} \in \mathbb{C}^{N_{\mathrm{p}}\times N_{\mathrm{p}}}$ weights the estimated pilot subcarriers based on their estimation accuracy [15], [29]. The estimated CPEs are used for de-rotating the received data subcarriers according to $\tilde{\mathbf{z}}_{\kappa,\gamma}^{\mathrm{d}} = \mathbf{z}_{\kappa,\gamma}^{\mathrm{d}} \cdot \mathrm{e}^{-\mathrm{j}\widehat{\varphi}_{\kappa,\gamma}}$.

E. DATA ESTIMATION

With $\tilde{\mathbf{z}}_\kappa^{\mathrm{d}} = [(\tilde{\mathbf{z}}_{\kappa,0}^{\mathrm{d}})^T, (\tilde{\mathbf{z}}_{\kappa,1}^{\mathrm{d}})^T, (\tilde{\mathbf{z}}_{\kappa,2}^{\mathrm{d}})^T, (\tilde{\mathbf{z}}_{\kappa,3}^{\mathrm{d}})^T]^T \in \mathbb{C}^{4N_{\mathrm{d}}}$, $\widehat{\mathbf{H}}^{\mathrm{d}} = [(\widehat{\mathbf{H}}_0^{\mathrm{d}})^T, (\widehat{\mathbf{H}}_1^{\mathrm{d}})^T, (\widehat{\mathbf{H}}_2^{\mathrm{d}})^T, (\widehat{\mathbf{H}}_3^{\mathrm{d}})^T]^T \in \mathbb{C}^{4N_{\mathrm{d}}\times N_{\mathrm{d}}}$, and $\mathbf{n}_\kappa^{\mathrm{d}} = [(\mathbf{n}_{\kappa,0}^{\mathrm{d}})^T, (\mathbf{n}_{\kappa,1}^{\mathrm{d}})^T, (\mathbf{n}_{\kappa,2}^{\mathrm{d}})^T, (\mathbf{n}_{\kappa,3}^{\mathrm{d}})^T]^T \in \mathbb{C}^{4N_{\mathrm{d}}}$, the connection between $\tilde{\mathbf{z}}_{\kappa,0}^{\mathrm{d}}, \cdots, \tilde{\mathbf{z}}_{\kappa,3}^{\mathrm{d}}$ and the data symbols in $\mathbf{x}_\kappa^{\mathrm{d}}$ is given by $\tilde{\mathbf{z}}_\kappa^{\mathrm{d}} = \widehat{\mathbf{H}}^{\mathrm{d}}\mathbf{x}_\kappa^{\mathrm{d}} + \mathbf{n}_\kappa^{\mathrm{d}}$ The LMMSE estimator for

$\mathbf{x}_\kappa^{\mathrm{d}}$ can be derived as [29], [30], [36]

$$\widehat{\mathbf{x}}_\kappa^{\mathrm{d}} = \left(\left(\widehat{\mathbf{H}}^{\mathrm{d}}\right)^H\widehat{\mathbf{H}}^{\mathrm{d}} + \frac{N_{\mathrm{c}}\sigma_{\mathrm{n}}^2}{\sigma_{\mathrm{d}}^2}\mathbf{I}^{N_{\mathrm{d}}}\right)^{-1}\left(\widehat{\mathbf{H}}^{\mathrm{d}}\right)^H\tilde{\mathbf{z}}_\kappa^{\mathrm{d}}, \qquad (23)$$

representing the final estimate of the data symbols. Note that the matrix to be inverted in (23) is a diagonal matrix, which is trivial to invert. Overall, the computational complexity for the methods presented in this section is comparable to those for RDMult.

V. BER PERFORMANCE COMPARISON

In this section, the BER performance of the proposed MISO OFDM system using DDM is compared with that of a SISO OFDM system and with that of MISO OFDM systems utilizing ESI, RDMult, and NeqDySI. For the latter one, it is assumed that the receiver knows the assignment of the subcarrier sets to the individual Tx antennas. All considered systems employ the system parameters listed in Table 1 except for the SISO OFDM system for which $N_{\mathrm{Tx}} = 1$. Additional processing blocks, e.g., the channel coder/decoder [29], [31], [37], the mapper/demapper [38], [39], [40], interleaver/deinterleaver, randomized CIR generation [18], [19], [20], [21], [22], [23], [24], correspond to those utilized in [15]. For each CIR, a relative velocity is drawn from a uniform distribution between ± 60 m/s. The effects of this relative velocity on the channel are modelled in form of ICI and a CPE [15], [29].

The simulations are carried out for fixed values of E_{b}/N_0, where E_{b} is the average energy per bit of information, and where $N_0/2$ is the double-sided noise power spectral density [29]. The noise variance σ_{n}^2 of the complex-valued AWGN at the receiver input is chosen according to [29], [41]

$$\sigma_{\mathrm{n}}^2 = \frac{P_{\mathrm{s}}}{(E_{\mathrm{b}}/N_0)br\zeta\nu}, \qquad (24)$$

where P_{s} is the average signal power per time-domain sample, b is the number of bits per data symbol, r denotes the code rate of the channel code, and $\zeta = N_{\mathrm{c}}/(N_{\mathrm{cp}} + N_{\mathrm{c}})$ accounts for the time domain samples in the CP. The parameter ν accounts for the additional redundancy discussed in Section IV. Thus, $\nu = \frac{1}{4}$ for the MISO OFDM system employing DDM. RDMult adds a similar redundancy [15], such that $\nu = \frac{1}{4}$ is chosen also for this system. All other considered systems do not add any additional redundancy such that $\nu = 1$ is chosen for them. As a result, MISO OFDM systems employing DDM and RDMult observe a higher noise variance σ_{n}^2.

A. PERFECT CHANNEL KNOWLEDGE; PERFECT SYNCHRONIZATION

In this first simulation, the receiver perfectly knows the channel between transmitter and receiver. The observed BER curves for uncoded and coded transmission are shown in Fig. 4. While for the uncoded case, RDMult has a small advantage in BER performance over DDM, both systems feature approximately the same BER performance in the coded case and outperform the remaining systems by approximately
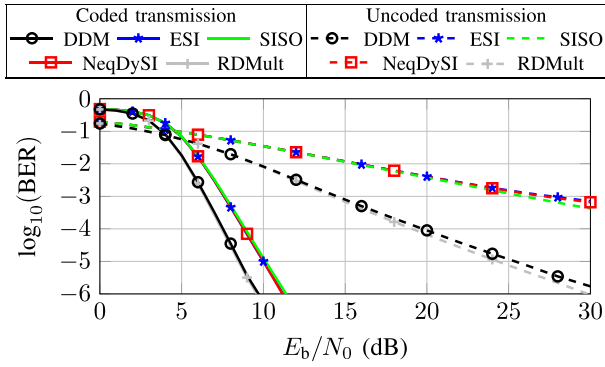
FIGURE 4. BER curves for the case of perfect synchronization and perfect channel knowledge. The solid lines are for coded, and the dashed lines are for uncoded transmission. The curves for DDM and RDMult as well as the curves for SISO, ESI, and NeqDySI almost lie on top of each other.
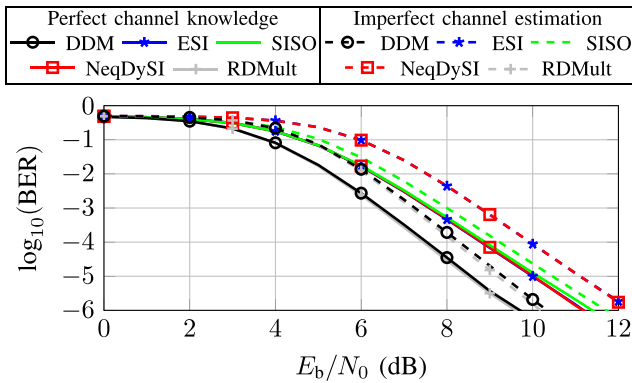

FIGURE 6. BER curves for the case of perfect channel knowledge, code rate $r = 1/2$, and perfect synchronization (solid) and for imperfect synchronization (dashed). The curves for DDM and RDMult as well as the curves for SISO, ESI, and NeqDySI almost lie on top of each other.

FIGURE 5. BER curves for the case of perfect synchronization, code rate $r = 1/2$, and perfect channel knowledge (solid) and for imperfect channel estimation (dashed).

1.6 dB. This gain in BER performance is a result of the diversity gain elaborated on in Section IV, whose origin is the transmission of the same subcarrier symbols on several consecutive OFDM symbols. The remaining simulations are shown for coded transmission only.

B. PERFECT SYNCHRONIZATION; IMPERFECT CHANNEL ESTIMATION BASED ON PREAMBLE OFDM SYMBOLS

Now, the channel is not perfectly known but rather estimated using the procedure derived in Section IV-C. The channels for the SISO OFDM system and the MISO OFDM systems utilizing ESI and NeqDySI are estimated with the BLUE [30], [32], [33]. For a fair comparison by means of having similar distortions on the channel estimates, all three systems shall have the same effective SNR for the averaged preamble OFDM symbols [15]. Hence, the increased noise variance σ_n^2 for the MISO OFDM systems with DDM and RDMult is compensated by employing $N_{pr} = 16$ preamble OFDM symbols, while the other systems use $N_{pr} = 4$.

The resulting BER curves are shown in Fig. 5. This figure also visualizes the simulation results for the case of perfect channel knowledge from Fig. 4 as reference. While the MISO
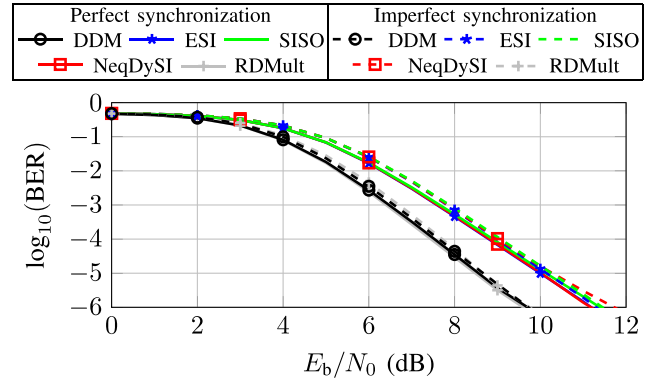
systems are less prone to imperfect channel knowledge, the loss in performance for all three systems is moderate. The systems utilizing RDMult and DDM outperform the other MISO systems by approximately 2 dB.

C. PERFECT CHANNEL KNOWLEDGE; IMPERFECT SYNCHRONIZATION USING PILOT SUBCARRIERS

For the case of perfect channel knowledge but imperfect synchronization, the SISO OFDM system and the MISO OFDM systems utilizing ESI and NeqDySI employ $N_p = 16$ pilot subcarriers. The MISO OFDM systems with DDM and RD-Mult employ $N_p = 64$ pilot subcarriers to ensure the same effective SNR as argued previously. The BER curves visualized in Fig. 6 show that the loss in BER performance is minor for all considered systems. The systems utilizing RDMult and DDM outperform the other MISO systems by approximately 1.7 dB.

VI. CONCLUSION

In this work, a thorough investigation of the properties of DDM on the communication aspects of OFDM joint sensing and communication systems has been carried out. We showed that the communication channel can be modelled by a so-called effective channel, which is a SISO channel although several Tx antennas are involved. This effective channel turned out to be heavily time-varying, entailing the necessity of countermeasures. We proposed a communication system specifically designed to cope with the time-varying nature of the channel including methods for data estimation, synchronization, and channel estimation, whose performances were evaluated through BER simulations.

REFERENCES

[1] O. B. Akan and M. Arik, "Internet of radars: Sensing versus sending with joint radar-communications," *IEEE Commun. Mag.*, vol. 58, no. 9, pp. 13–19, Sep. 2020.

[2] D. Ma, N. Shlezinger, T. Huang, Y. Liu, and Y. C. Eldar, "Joint radar-communication strategies for autonomous vehicles: Combining two key automotive technologies," *IEEE Signal Process. Mag.*, vol. 37, no. 4, pp. 85–97, Jul. 2020.

[3] C. Waldschmidt and H. Meinel, "Future trends and directions in radar concerning the application for autonomous driving," in *Proc. IEEE Eur. Radar Conf.*, 2014, pp. 416–419.

[4] C. Sturm, E. Pancera, T. Zwick, and W. Wiesbeck, "A novel approach to OFDM radar processing," in *Proc. IEEE Radar Conf.*, 2009, pp. 1–4.

[5] C. Sturm, T. Zwick, and W. Wiesbeck, "An OFDM system concept for joint radar and communications operations," in *Proc. IEEE Veh. Technol. Conf.*, 2009, pp. 1–5.

[6] Y. L. Sit and T. Zwick, "Automotive MIMO OFDM radar: Subcarrier allocation techniques for multiple-user access and DOA estimation," in *Proc. Eur. Radar Conf.*, 2014, pp. 153–156.

[7] G. Hakobyan and B. Yang, "A novel OFDM-MIMO radar with non-equidistant subcarrier interleaving and compressed sensing," in *Proc. Int. Radar Symp.*, 2016, pp. 1–5.

[8] G. Hakobyan and B. Yang, "A novel inter-carrier-interference free signal processing scheme for OFDM radar," *IEEE Trans. Veh. Technol.*, vol. 67, no. 6, pp. 5158–5167, Jun. 2018.

[9] B. Nuss, J. Mayer, and T. Zwick, "Limitations of MIMO and multi-user access for OFDM radar in automotive applications," in *Proc. IEEE MTT-S Int. Conf. Microw. Intell. Mobility*, 2018, pp. 1–4.

[10] C. Sturm, Y. L. Sit, M. Braun, and T. Zwick, "Spectrally interleaved multi-carrier signals for radar network applications and multi-input multi-output radar," *IET Radar Sonar Navig.*, vol. 7, no. 3, pp. 261–269, 2013.

[11] C. Knill, F. Roos, B. Schweizer, D. Schindler, and C. Waldschmidt, "Random multiplexing for an MIMO-OFDM radar with compressed sensing-based reconstruction," *IEEE Microw. Wireless Compon. Lett.*, vol. 29, no. 4, pp. 300–302, Apr. 2019.

[12] G. Hakobyan and B. Yang, "A novel OFDM-MIMO radar with non-equidistant dynamic subcarrier interleaving," in *Proc. IEEE Eur. Radar Conf.*, 2016, pp. 45–48.

[13] C. Knill, F. Embacher, B. Schweizer, S. Stephany, and C. Waldschmidt, "Coded OFDM waveforms for MIMO radars," *IEEE Trans. Veh. Technol.*, vol. 70, no. 9, pp. 8769–8780, Sep. 2021.

[14] J. Suh, J. Lee, G.-T. Gil, and S. Hong, "Time-and-frequency hybrid multiplexing for flexible ambiguity controls of DFT-coded MIMO OFDM radar," *IEEE Access*, vol. 9, pp. 137793–137808, 2021.

[15] O. Lang, C. Hofbauer, R. Feger, and M. Huemer, "Range-division multiplexing for MIMO OFDM joint radar and communications," *IEEE Trans. Veh. Technol.*, vol. 72, no. 1, pp. 52–65, Jan. 2023.

[16] R. van Nee and R. Prasad, *OFDM for Wireless Multimedia Communications*. Norwood, MA, USA: Artech House, 2000.

[17] S. M. Patole, M. Torlak, D. Wang, and M. Ali, "Automotive radars: A review of signal processing techniques," *IEEE Signal Process. Mag.*, vol. 34, no. 2, pp. 22–35, Mar. 2017.

[18] M. K. Samimi and T. S. Rappaport, "Statistical channel model with multi-frequency and arbitrary antenna beamwidth for millimeter-wave outdoor communications," in *Proc. IEEE Globecom Workshops*, 2015, pp. 1–7.

[19] M. K. Samimi and T. S. Rappaport, "3-D millimeter-wave statistical channel model for 5G wireless system design," *IEEE Trans. Microw. Theory Techn.*, vol. 64, no. 7, pp. 2207–2225, Jul. 2016.

[20] S. Ju, O. Kanhere, Y. Xing, and T. S. Rappaport, "A millimeter-wave channel simulator NYUSIM with spatial consistency and human blockage," in *Proc. IEEE Glob. Commun. Conf.*, 2019, pp. 1–6.

[21] S. Sun, G. R. MacCartney, and T. S. Rappaport, "A novel millimeter-wave channel simulator and applications for 5G wireless communications," in *Proc. IEEE Int. Conf. Commun.*, 2017, pp. 1–7.

[22] S. Sun, T. S. Rappaport, M. Shafi, P. Tang, J. Zhang, and P. J. Smith, "Propagation models and performance evaluation for 5G millimeter-wave bands," *IEEE Trans. Veh. Technol.*, vol. 67, no. 9, pp. 8422–8439, Sep. 2018.

[23] T. S. Rappaport, S. Sun, and M. Shafi, "Investigation and comparison of 3GPP and NYUSIM channel models for 5G wireless communications," in *Proc. IEEE Veh. Technol. Conf.*, 2017, pp. 1–5.

[24] N. WIRELESS, "Open source downloadable 5G channel simulator software," 2017, Accessed: Aug. 2020. [Online]. Available: http://bit.ly/1WNPpDX

[25] B. Lu and X. Wang, "Space-time code design in OFDM systems," in *Proc. IEEE Glob. Telecommun. Conf.*, 2000, pp. 1000–1004.

[26] S. M. Alamouti, "A simple transmit diversity technique for wireless communications," *IEEE J. Sel. Areas Commun.*, vol. 16, no. 8, pp. 1451–1458, Oct. 1998.

[27] V. Tarokh, N. Seshadri, and A. R. Calderbank, "Space-time codes for high data rate wireless communication: Performance criterion and code construction," *IEEE Trans. Inf. Theory*, vol. 44, no. 2, pp. 744–765, Mar. 1998.

[28] F. Classen and H. Meyr, "Frequency synchronization algorithms for OFDM systems suitable for communication over frequency selective fading channels," in *Proc. IEEE Veh. Technol. Conf.*, 1994, pp. 1655–1659.

[29] C. Hofbauer, "Design and analysis of unique word OFDM," Ph.D. thesis conducted at the Institute of Networked and Embedded Systems, Alpen-Adria-University Klagenfurt, Klagenfurt, Austria, 2016. [Online]. Available: https://permalink.obvsg.at/UKL/AC12608830

[30] S. M. Kay, *Fundamentals of Statistical Signal Processing: Estimation Theory*, vol. 1. Hoboken, NJ, USA: Prentice Hall, 1993.

[31] M. Salehi and J. Proakis, *Digital Communications*. New York, NY, USA: McGraw-Hill Educ., 2007.

[32] M. Huemer and O. Lang, "On component-wise conditionally unbiased linear Bayesian estimation," in *Proc. Asilomar Conf. Signals, Syst., Comput.*, 2014, pp. 879–885.

[33] O. Lang, "Knowledge-aided methods in estimation theory and adaptive filtering," Ph.D. thesis conducted at the Institute of Signal Processing, Johannes Kepler University Linz, Linz, Austria, 2018.

[34] C. Hofbauer, W. Haselmayr, H.-P. Bernhard, and M. Huemer, "Impact of a carrier frequency offset on unique word OFDM," in *Proc. Int. Symp. Pers., Indoor Mobile Radio Commun.*, London, U.K., 2020, pp. 1–7.

[35] C. Hofbauer, W. Haselmayr, H.-P. Bernhard, and M. Huemer, "On the inclusion and utilization of pilot tones in unique word OFDM," *IEEE Trans. Signal Process.*, vol. 68, pp. 5504–5518, 2020.

[36] M. Huemer, A. Onic, and C. Hofbauer, "Classical and Bayesian linear data estimators for unique word OFDM," *IEEE Trans. Signal Process.*, vol. 59, no. 12, pp. 6073–6085, Dec. 2011.

[37] A. Viterbi, "Error bounds for convolutional codes and an asymptotically optimum decoding algorithm," *IEEE Trans. Inf. Theory*, vol. 13, no. 2, pp. 260–269, Apr. 1967.

[38] S. Allpress, C. Luschi, and S. Felix, "Exact and approximated expressions of the log-likelihood ratio for 16-QAM signals," in *Proc. IEEE Asilomar Conf. Signals, Syst., Comput.*, 2004, pp. 794–798.

[39] W. Haselmayr, O. Lang, A. Springer, and M. Huemer, "Does vector Gaussian approximation after LMMSE filtering improve the LLR quality?," *IEEE Signal Process. Lett.*, vol. 24, no. 11, pp. 1676–1680, Nov. 2017.

[40] O. Lang, M. Huemer, and C. Hofbauer, "On the log-likelihood ratio evaluation of CWCU linear and widely linear MMSE data estimators," in *Proc. Asilomar Conf. Signals, Syst., Comput.*, 2016, pp. 633–637.

[41] W. Zhang and M. J. Miller, "Baseband equivalents in digital communication system simulation," *IEEE Trans. Educ.*, vol. 35, no. 4, pp. 376–382, Nov. 1992.